MIZ1 regulates ECA1 to generate a slow, long-distance phloem-transmitted Ca^{2+} signal essential for root water tracking in *Arabidopsis*

Doron Shkolnik[a], Roye Nuriel[a], Maria Cristina Bonza[b], Alex Costa[b,c], and Hillel Fromm[a,1]

[a]School of Plant Sciences and Food Security, Faculty of Life Sciences, Tel Aviv University, Tel Aviv 69978, Israel; [b]Department of Biosciences, University of Milan, 20133 Milan, Italy; and [c]Institute of Biophysics, Consiglio Nazionale delle Ricerche, 20133 Milan, Italy

Edited by Jian-Kang Zhu, Purdue University, West Lafayette, IN, and approved June 27, 2018 (received for review March 9, 2018)

Ever since Darwin postulated that the tip of the root is sensitive to moisture differences and that it "transmits an influence to the upper adjoining part, which bends towards the source of moisture" [Darwin C, Darwin F (1880) *The Power of Movement in Plants*, pp 572–574], the signal underlying this tropic response has remained elusive. Using the FRET-based Cameleon Ca^{2+} sensor *in planta*, we show that a water potential gradient applied across the root tip generates a slow, long-distance asymmetric cytosolic Ca^{2+} signal in the phloem, which peaks at the elongation zone, where it is dispersed laterally and asymmetrically to peripheral cells, where cell elongation occurs. In addition, the MIZ1 protein, whose biochemical function is unknown but is required for root curvature toward water, is indispensable for generating the slow, long-distance Ca^{2+} signal. Furthermore, biochemical and genetic manipulations that elevate cytosolic Ca^{2+} levels, including mutants of the endoplasmic reticulum (ER) Ca^{2+}-ATPase isoform ECA1, enhance root curvature toward water. Finally, coimmunoprecipitation of plant proteins and functional complementation assays in yeast cells revealed that MIZ1 directly binds to ECA1 and inhibits its activity. We suggest that the inhibition of ECA1 by MIZ1 changes the balance between cytosolic Ca^{2+} influx and efflux and generates the cytosolic Ca^{2+} signal required for water tracking.

MIZ1 | ECA1 | hydrotropism | calcium | *Arabidopsis*

Plant adaptation to environmental changes requires continuous foraging for water to survive. Roots have evolved a yet-unexplained mechanism that directs their growth toward high water potential, a task that requires overcoming their default growth pattern along the gravity vector (gravitropism) (1–3). Landmark experiments demonstrated the importance of the root cap in sensing moisture and directing growth toward the water source (1, 4). If this is indeed the case, then numerous questions need to be addressed to elucidate the mechanism underlying hydrotropism: First, how is the water gradient detected; second, following the sensing, how does the detector transduce the sense to a signal, which is transmitted from the root cap to the elongation zone (EZ); third, which asymmetric cross-root signal underlies differential growth across the root, resulting in root bending toward the water source? Although it has been shown that the osmotic stress hormone abscisic acid (ABA) is required for hydrotropism (5, 6), there is no evidence for ABA signaling from the root cap to the EZ, nor is there evidence for the asymmetric distribution of ABA across the root in response to moisture gradients (6). The requirement of the hormone auxin, a regulator of some tropic responses (7–9), was revoked in relation to hydrotropism because it is not asymmetrically distributed following hydrostimulation (10, 11). Moreover, blocking of auxin polar transport, or TIR-dependent auxin signaling, enhanced hydrotropism (10, 11). Interestingly, reactive oxygen species (ROS) play an important role in tuning root tropic responses by acting positively in gravitropism and negatively in hydrostimulation (12, 13). In recent years, accumulating evidence has suggested that Ca^{2+} plays a key role in long-distance, systemic signaling in response to various stress stimuli (14, 15), for example, mediating the occlusion of phloem sieve tube elements in response to wounding (16), evoking electric signaling (15), and mediating rapid Ca^{2+} waves in roots responding to salt stress (14). Moreover, since both ABA and ROS signaling interact with Ca^{2+} signaling in plants, and since Ca^{2+} was suggested to be involved both in hydrotropic and gravitropic responses (17–20) and in cell elongation in different plant tissues (21, 22), we sought to assess the possible role of Ca^{2+} as a signal from the root cap to the EZ for root bending upon hydrostimulation.

Results

An MIZ1-Dependent Slow Shootward Cytosolic Ca^{2+} Signal Is Required for Root Hydrotropism. To analyze cytosolic Ca^{2+} ($[Ca^{2+}]_{cyt}$) levels in the roots of wild-type (WT) *Arabidopsis* (Col-0), transgenic plants that express the cytosol-targeted, FRET-based Ca^{2+} sensor Cameleon (NES-YC3.6) (23) were studied by confocal microscopy. Confocal visualization of the NES-YC3.6 ratio intensity in Col-0 roots under control conditions revealed high levels of $[Ca^{2+}]_{cyt}$ at the columella, meristematic zone, lateral root cap, and the EZ vasculature (Fig. 1*A*). Strikingly, following 1 h of hydrostimulation in a split-agar/sorbitol system (*Materials and Methods*), $[Ca^{2+}]_{cyt}$ levels were elevated at the root tip (Fig. 1*A* and *SI Appendix*, Fig. S1*A*) and at the vasculature of the meristem and elongation zones, with an apparent asymmetric distribution at the EZ, where higher $[Ca^{2+}]_{cyt}$ levels were observed at the side that becomes

Significance

Plant roots grow toward water, a phenomenon termed hydrotropism. The nature of the root signal that governs hydrotropism is elusive and remains to be elucidated. Here, we show that, in response to water potential differences across the root tip, a slow, asymmetric long-distance Ca^{2+} signal is transmitted via the phloem to the elongation zone, where it is asymmetrically distributed across the root to promote root curvature. Furthermore, we demonstrate that the hydrotropism-associated protein MIZ1 plays a role in generating the Ca^{2+} signal by its direct binding to and inhibition of ECA1, an endoplasmic reticulum Ca^{2+} pump, which resembles the animal sarco/endoplasmic reticulum Ca^{2+}-ATPases (SERCAs). This study elucidates the mechanism underlying systemic Ca^{2+} signaling in plant roots, which is essential for water tracking.

Author contributions: D.S., M.C.B., A.C., and H.F. designed research; D.S., R.N., M.C.B., and A.C. performed research; R.N. contributed new reagents/analytic tools; D.S., M.C.B., A.C., and H.F. analyzed data; and D.S., M.C.B., A.C., and H.F. wrote the paper.

The authors declare no conflict of interest.

This article is a PNAS Direct Submission.

[1]To whom correspondence should be addressed. Email: hillelf@post.tau.ac.il.

This article contains supporting information online at www.pnas.org/lookup/suppl/doi:10.1073/pnas.1804130115/-/DCSupplemental.

Published online July 16, 2018.

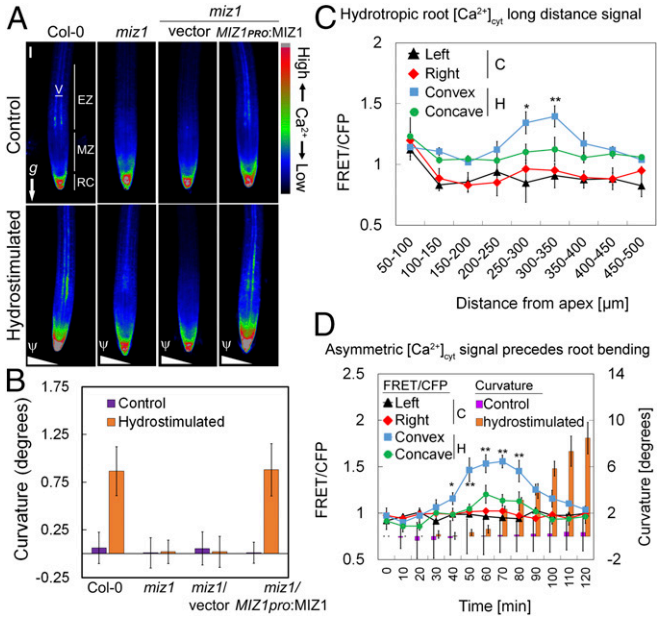

Fig. 1. Asymmetric MIZ1-mediated $[Ca^{2+}]_{cyt}$ signal is required for root tip response to moisture gradient. (*A*) NES-YC3.6 confocal microscopy visualization in roots of Col-0, *miz1*, *miz1*/empty pPZP RCS2 BAR (vector), and *miz1*/*MIZ1pro*:MIZ1 seedlings. FRET/CFP-based images were pseudocolored, where red indicates higher $[Ca^{2+}]_{cyt}$ levels. EZ, elongation zone; MZ, meristematic zone; RC, root cap; V, vasculature. *g* represents gravity vector, and Ψ represents water potential gradient. (Scale bar, 50 μm.) (*B*) Measurements of root curvature following control or 1 h of hydrostimulation. (*C*) Quantification of FRET/CFP intensity ratio of two longitudinal halves of 50-μm root segments, 50–500 μm above the apex of NES-YC3.6–expressing Col-0 seedlings. (*D*) Quantification of FRET/CFP intensity ratio (lines) of the two longitudinal halves of the EZ (250–350 μm above apex) of control and 1-h–hydrostimulated NES-YC3.6–expressing Col-0 seedlings. Curvature (columns) was measured at each time point. In *C* and *D*, C, control; H, hydrostimulated. Error bars represent mean ± SD (three biological independent experiments; 10 seedlings each); $*P < 0.01$, $**P < 0.001$, Student's *t* test versus FRET/CFP value measured in the concave side.

convex upon bending (Fig. 1*A* and Movies S1 and S2). This result was also reproduced using a split-agar/mannitol system (*SI Appendix*, Fig. S2), indicating that the $[Ca^{2+}]_{cyt}$ elevation is not a specific response to sorbitol. To further assess the relationship between the long-distance Ca^{2+} signal and the cellular pathways mediating root curvature to moisture, we visualized $[Ca^{2+}]_{cyt}$ in mutants of the *Mizu-Kussey 1* (*MIZ1*) gene, which encodes an ER membrane-associated protein (24, 25), whose biochemical or cellular functions are unknown but is indispensable for root curvature in response to moisture gradients (24). Analysis of the $[Ca^{2+}]_{cyt}$ distribution along the root tip of control and hydrostimulated *miz1* mutants harboring the Cameleon Ca^{2+} sensor revealed lower basal $[Ca^{2+}]_{cyt}$ levels under control conditions, which were not elevated nor asymmetrically distributed at the EZ following hydrostimulation (Fig. 1*A*, *SI Appendix*, Fig. S3, and Movie S3), suggesting that a functional MIZ1 is required for generating the long-distance Ca^{2+} signal in response to hydrostimulation. Indeed, the expression of an active MIZ1 (under the transcriptional regulation of the native *MIZ1* promoter) in the *miz1*/NES-YC3.6 plants fully restored the $[Ca^{2+}]_{cyt}$ signal and root bending (Fig. 1 *A* and *B*). These results identified MIZ1 as a cellular component in mediating Ca^{2+} signaling in response to hydrostimulation. Since MIZ1 is associated with the ER membrane (25), we also examined whether Ca^{2+} levels in the ER ($[Ca^{2+}]_{ER}$) might be altered in hydrostimulated root tips by analyzing *Arabidopsis* plants expressing the ER localized CRT-D4ER Cameleon sensor (26). Interestingly, $[Ca^{2+}]_{ER}$ significantly decreases in hydrostimulated root tips in parallel with the elevation in $[Ca^{2+}]_{Cyt}$ (*SI Appendix*, Fig. S1). These data strongly suggest that, in root tip cells, the ER serves as a Ca^{2+} reservoir that functions in generating the hydrotropic $[Ca^{2+}]_{cyt}$ signal.

Cameleon ratiometric analysis from the meristem to the EZ (50–500 μm above apex) in two sides of control and hydrostimulated Col-0 and *miz1* roots revealed the formation of a statistically significant asymmetric $[Ca^{2+}]_{cyt}$ distribution at ∼250- to 400-μm segment above the root apex of the EZ of hydrostimulated Col-0, which was not observed in control Col-0 roots nor in control or hydrostimulated *miz1* roots (Fig. 1*C*, *SI Appendix*, Fig. S3*A*, and Movies S1–S3). This relatively slow, long-distance signaling pattern, occurring in the range of an hour, is distinct in its kinetics and tissue specificity from previously reported Ca^{2+} waves or propagations in response to abiotic or biotic stimuli that occur in seconds to minutes (14, 27, 28).

Next, we determined whether the kinetics of the asymmetric distribution of $[Ca^{2+}]_{cyt}$ coincides with the root bending time course by measuring the NES-YC3.6 signal at the EZ and the root bending every 10 min, 0–120 min from the start of hydrostimulation. In Col-0, the results show a maximum difference of $[Ca^{2+}]_{cyt}$ across the root EZ at about 50–80 min from the onset of hydrostimulation, with an estimated $[Ca^{2+}]_{cyt}$ peak of 244.5 ± 22 nM (conversion of the FRET/CFP ratio value to molar concentration was performed as in ref. 20) at the forming convex side following 70 min, whereas significant curvature toward higher water potential was observed after about 60–70 min (Fig. 1*D*). No asymmetric signal was apparent in *miz1* roots in which $[Ca^{2+}]_{cyt}$ levels did not rise above ∼102.9 ± 15 nM in either root side at any time point during 120 min of hydrostimulation (*SI Appendix*, Fig. S3*B*). These data clearly show that $[Ca^{2+}]_{cyt}$ elevation and its asymmetric distribution at the EZ of the root precede root bending and thus most likely regulate it in a mechanism requiring the activity of MIZ1.

To determine whether the asymmetric $[Ca^{2+}]_{cyt}$ signal across the root indeed results from an asymmetric water potential distribution at the root tip, rather than a general, or predisposed response to osmotic stress, we compared the kinetics of the distribution of $[Ca^{2+}]_{cyt}$ across the root in a diagonal split-agar/sorbitol system, with that caused by a horizontal split-agar/sorbitol system (Fig. 2*A*). After 30 min of stimulation, an asymmetric Ca^{2+} signal was observed in the diagonal split-agar/sorbitol assay. In contrast, no asymmetric $[Ca^{2+}]_{cyt}$ signal was observed in Col-0 roots even after 1 h of hydrostimulation in the horizontal split-agar/sorbitol system (Fig. 2*B*). Moreover, the direction of root bending in the diagonal system was unified toward high water potential, whereas following stimulation in the

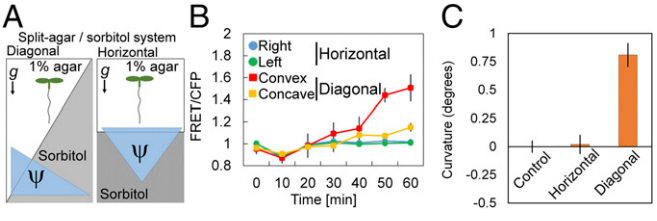

Fig. 2. Asymmetric $[Ca^{2+}]_{cyt}$ signal in the root tip is generated in response to exposure to asymmetric water potential gradient. (*A*) Schematic presentation of horizontal and diagonal hydrostimulation assay systems. *g* represents gravity vector, and Ψ represents water potential gradient. (*B* and *C*) Quantification of FRET/CFP intensity ratio (*B*) and root curvature (*C*) of two longitudinal halves of the EZ (250–350 μm above apex) of NES-YC3.6–expressing Col-0 seedlings hydrostimulated for the indicated times, using the two systems depicted in *A*. In *B* and *C*, error bars represent mean ± SD (three biological independent experiments, 10 seedlings each).

horizontal system, nonunified root growth direction was observed (Fig. 2*C*). These data indicate that the formation of the asymmetric $[Ca^{2+}]_{cyt}$ signal directly results from root tip exposure to asymmetric water potential. In contrast, examination of the $[Ca^{2+}]_{cyt}$ in gravistimulated roots revealed no generation of a Ca^{2+} signal along the root, before or after an observed root curvature (*SI Appendix*, Fig. S4), in agreement with previous findings (17). Thus, the slow, asymmetric Ca^{2+} signal from the root tip to the EZ is a specific response to water potential distribution across the root. Collectively, these data, obtained in intact roots, strongly support the importance of the root cap and meristem in perceiving changes in water potential pressure and in generating a Ca^{2+} signal transmitted to the EZ to promote bending, as also suggested in previous studies (1, 4).

The Shootward Asymmetric Ca^{2+} Signal Is Transmitted Through the Root Phloem to the EZ Where It Is Laterally and Asymmetrically Distributed Across the Root. To pinpoint the specific vascular tissue in which the slow, long-distance Ca^{2+} signal is transmitted, we visualized the NES-YC3.6 fluorescence ratio (signal intensity) in the background of the bright-field images of root segments from two perspective angles relative to the phloem and xylem poles (Fig. 3*A*). To optimize the resolution of our visual inspection, we adjusted the maximum and minimum ratio values such that the cells with the highest signal intensity could be identified. Clearly, when the ratio signal in the protoxylem was found to be below the intensity cutoff, a prominent continuous longitudinal $[Ca^{2+}]_{cyt}$ signal was visualized in the phloem tissue (Fig. 3*A*), a result that is in agreement with previous reports of Ca^{2+} transport and function in phloem sieve tubes in response to osmotic or biotic stresses (16, 29).

If indeed the asymmetric Ca^{2+} increase in the EZ vasculature (phloem) regulates root bending, it should either reach the cells of the peripheral layers (e.g., cortex) by lateral mobilization, where differential elongation takes place, or it should be conveyed to the peripheral cells by a different signal. To address this issue, we used light-sheet fluorescence microscopy to visualize the radial root EZ of NES-YC3.6–expressing seedlings upon hydrostimulation (30). For this purpose, we designed a special "in-tube" hydrostimulation system (Fig. 3*B*). Under control conditions, we found the highest $[Ca^{2+}]_{cyt}$ level in phloem cells and much less in peripheral tissue layers, mainly at the phloem pole outer layers, with no apparent asymmetry (Fig. 3 *C* and *D*). Strikingly, in hydrostimulated roots, $[Ca^{2+}]_{cyt}$ levels were elevated in the peripheral tissues, with substantially higher levels in the phloem and cortex of the evolving convex root side (Fig. 3 *C* and *D*). Interestingly, lateral Ca^{2+} mobilization, possibly through plasmodesmata (31, 32), from phloem sieve tubes to peripheral tissues, was previously proposed (16). Collectively, these data strongly suggest that, in response to asymmetric water potential distribution across the root tip, an asymmetric long-distance Ca^{2+} signal spreads via the phloem, followed by lateral Ca^{2+} mobilization to peripheral cells at the EZ, required for differential root elongation and bending. Nevertheless, how Ca^{2+} at the EZ affects differential cell elongation remains an open question.

Elevation of $[Ca^{2+}]_{cyt}$ in the Root Is Essential for Hydrotropic Bending. To test the effect of Ca^{2+} on the root's tropic response to moisture distribution, we treated wild-type (Col-0) plants with the highly selective, cell-permeant Ca^{2+} chelator 1,2-bis(2-aminophenoxy)ethane-*N*,*N*,*N*′,*N*′-tetraacetic acid tetrakis–acetoxymethyl ester (BAPTA-AM) before hydrostimulation using the split-agar/sorbitol system. Control plants (without BAPTA-AM) displayed normal root bending, as described in a similar published experimental setup (13, 33, 34), whereas BAPTA-AM–treated roots displayed arrested bending in response to the change in water potential in their microenvironment even after 12 h, while continuing their growth toward the sorbitol-containing media (Fig. 4 *A* and *B*). In contrast, pretreatment of seedlings with the Ca^{2+} ionophore, Br-A23187, significantly enhanced root curvature by up to ∼50% more than in control roots (Fig. 4 *C* and *D*). The effectiveness of BAPTA-AM and Br-A23187 treatments on $[Ca^{2+}]_{cyt}$ levels before hydrostimulation was monitored in roots of NES-YC3.6–expressing seedlings, and it was found to reduce and elevate $[Ca^{2+}]_{cyt}$ levels, respectively (*SI Appendix*, Fig. S5 *A* and *B*), as expected. In addition, these treatments were not found to significantly affect root growth under normal conditions (*SI Appendix*, Fig. S5*B*). These data suggest that the tropic response of *Arabidopsis* roots to a water potential gradient requires the elevation of $[Ca^{2+}]_{cyt}$ levels.

To corroborate the effect of $[Ca^{2+}]_{cyt}$ in roots responding to water potential gradients, mutants with aberrations in type 2B Ca^{2+} pumps, including ACA2 (AT4G37640), ACA8 (AT5G57110), and ACA10 (AT4G29900), were subjected to hydrostimulation in the

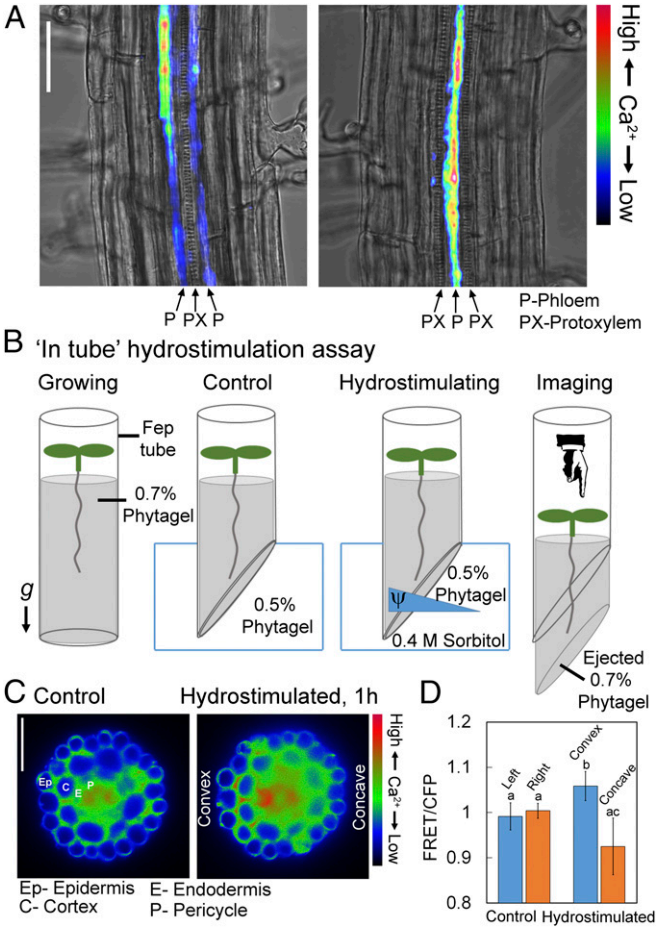

Fig. 3. $[Ca^{2+}]_{cyt}$ signal is transmitted via the root phloem to form an asymmetric lateral Ca^{2+} gradient in response to hydrostimulation. (*A*) Confocal microscope visualization of NES-YC3.6 EZ of Col-0 roots from two perspective angles relative to the xylem and phloem poles. The maximum and minimum FRET/CFP ratio values were adjusted so that the cells with the highest signal could be identified by superimposing the ratio images on bright-field images. (Scale bar, 50 μm.) (*B*) Schematic presentation of the in-tube hydrostimulation assay designed for root imaging using light-sheet fluorescence microscopy. (*C*) Visualization of radial EZ root sections of control and hydrostimulated NES-YC3.6–expressing Col-0 seedlings treated as in *B*. (Scale bar, 50 μm.) Images were created based on FRET/CFP ratio and pseudocolored when red indicates higher $[Ca^{2+}]_{cyt}$. (*D*) Quantification of the FRET/CFP intensity ratio of control and hydrostimulated roots radial halves that were obtained as in *B*. Error bars represent mean ± SD (three biological experiments; five seedlings each). Bars with different letters represent statistically different values by Tukey's HSD post hoc test ($P < 0.01$).

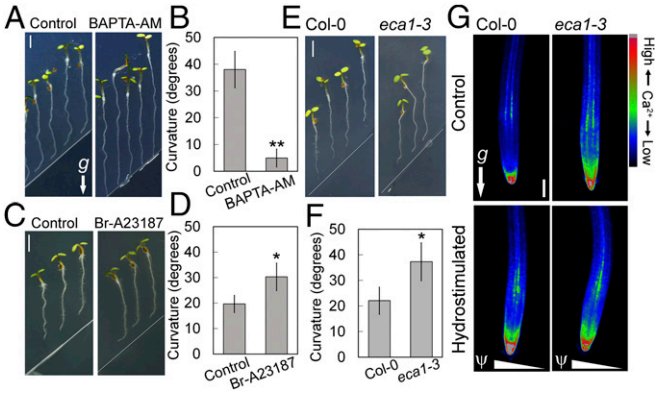

Fig. 4. Cytosolic Ca^{2+} levels determine root tip response to moisture gradient. (*A*, *C*, and *E*) Split-agar/sorbitol system to determine root curvature in response to hydrostimulation (*SI Appendix, Materials and Methods*). (*A–D*) Wild-type *Arabidopsis* (Col-0) seedlings were treated for 2 h with the cell-permeant Ca^{2+} chelator BAPTA-AM (10 μM) or the ionophore Br-A23187 (20 μM) before 12 or 6 h of hydrostimulation (*SI Appendix, Materials and Methods*), respectively, and curvature was scored. (*E* and *F*) *eca1-3* seedlings (versus Col-0 as control) were hydrostimulated for 6 h, and curvature was scored. In *B*, *D*, and *F*, error bars represent mean ± SD (three biological independent experiments, 10 seedlings each); $*P < 0.01$ and $**P < 0.005$, Student's *t* test versus control (*B* and *D*) or Col-0 (*F*). (*G*) Confocal microscope visualization of NES-YC3.6 signals in root tips of Col-0 and *eca1-3* under control conditions and following 1 h of hydrostimulation. Images were created based on FRET/CFP ratio and pseudocolored; red indicates higher $[Ca^{2+}]_{cyt}$ level. *g* represents gravity vector, and Ψ represents water potential gradient. (Scale bar, 50 μm.) All hydrostimulation assays were performed using the split-agar/sorbitol system.

split-agar/sorbitol system. None of the tested mutants exhibited appreciable differences from WT in root bending in response to hydrostimulation. On the other hand, mutant seedlings of the type 2A Ca^{2+}-ATPase ECA1, a pump that imports Ca^{2+} into the ER lumen (35), and which is related to the mammalian sarco/ER Ca^{2+}-ATPase (SERCA Ca^{2+} pump) (36), displayed enhanced bending toward higher water potential (Fig. 4 *E* and *F*). The growth rate of *eca1* roots was similar to that of the WT roots (*SI Appendix*, Fig. S5*D*).

In view of the known association of MIZ1 with the ER membrane (25), we pursued investigating ECA1 and MIZ1 regarding Ca^{2+} signaling, water tracking, and their possible interaction. Visualization of $[Ca^{2+}]_{cyt}$ in NES-YC3.6–expressing Col-0 and *eca1-3* roots under control and hydrostimulation conditions revealed higher concentrations of $[Ca^{2+}]_{cyt}$ in *eca1-3* than in Col-0 under both conditions (Fig. 4*G*) and an enhanced $[Ca^{2+}]_{cyt}$ signal following 1 h of hydrostimulation (*SI Appendix*, Fig. S6), which most likely explains the rapid response of *eca1* to hydrostimulation. Interestingly, examining the expression pattern of ECA1 in $ECA1_{pro}$:ECA1-GFP (in the genetic background of *eca1-1*) revealed ECA1 expression in all root tip tissues, with a higher abundance in the region between the apex and the EZ, and particularly high expression in the phloem (*SI Appendix*, Fig. S7 *A* and *B*). Measuring the hydrotropic root bending of $ECA1_{pro}$:*ECA1-GFP*-harboring *eca1-1* seedlings indicated full restoration of the normal tropic response (*SI Appendix*, Fig. S7*C*). These data suggest that inhibition of ECA1 may be required for generating the phloem-transmitted long-distance $[Ca^{2+}]_{cyt}$ signal in response to hydrostimulation.

MIZ1 Directly Interacts with ECA1 and Regulates Its Activity. To further study the possible involvement of ECA1 and MIZ1 in generating the $[Ca^{2+}]_{cyt}$ signal, we visualized the NES-YC3.6 ratios in Col-0 and *miz1* roots following treatment with cyclopiazonic acid (CPA), which was previously found to inhibit the *Arabidopsis* ECA1 (35). CPA treatment for 1 h elevated the $[Ca^{2+}]_{cyt}$ levels in Col-0 (in accordance with ref. 26) but not in *miz1* roots. This indicates that MIZ1 is required for CPA-mediated inhibition of ECA1 (Fig. 5*A*), possibly by direct interaction of MIZ1 with ECA1 or with an ECA1-associated protein complex. To further explore this possibility, we performed immunoprecipitation assays to isolate MIZ1-interacting proteins by using a GFP isolation kit to trap MIZ1-citrine or miz1-citrine from extracts of the corresponding transgenic plants. Interestingly, Western blot analysis of MIZ1-associated proteins indicated that ECA1 was indeed precipitated with MIZ1-citrine, but to a significantly lesser extent with miz1-citrine (Fig. 5 *B* and *C*), suggesting that ECA1 interacts with active MIZ1 in vivo (either directly or within a protein complex). To determine whether ECA1 and MIZ1 interact directly, we expressed ECA1 fused to the C terminus of ubiquitin (Cub) and MIZ1 or miz1 fused to the N terminus (Nub) to perform split-ubiquitin yeast two-hybrid assays. Remarkably, direct interaction of ECA1 with MIZ1, but not with miz1, was observed in this system (Fig. 5*D*). Expression of ECA1, MIZ1, and miz1 in yeast was confirmed using Western blot analysis (*SI Appendix*, Fig. S8*A*). In addition, to study the possible effect of MIZ1 on ECA1 function, we performed complementation analysis in which ECA1 was expressed alone or was coexpressed with MIZ1 or miz1 in the yeast K616 triple mutant, which lacks functional endogenous Ca^{2+}-dependent ATPases and is thus unable to grow on a Ca^{2+}-depleted medium (37). All transformants grew similarly on nonselective medium (10 mM Ca^{2+}) (Fig. 5*E*). Functional complementation assays on selective media (100 μM Ca^{2+} or even 20 mM EGTA, which reduces the free Ca^{2+} concentration in the medium to the nanomolar range), showed that expression of the *Arabidopsis* ECA1 alone completely restored yeast growth and complemented the K616 phenotype (Fig. 5*E*), as previously described (35, 38). Remarkably, coexpression of ECA1 with MIZ1 substantially reduced yeast growth under these selective conditions, suggesting an inhibitory effect of MIZ1 on ECA1. To assess the specificity of ECA1 inhibition by MIZ1, ECA1 was coexpressed with the miz1 mutant (Fig. 5*E*), which binds weakly to ECA1 both in yeast and in plant-derived microsomes (Fig. 5 *B–D*). Indeed, the growth of yeast coexpressing ECA1 with the miz1 mutant was much less inhibited compared with the growth of yeast expressing the WT proteins. Western blot analysis confirmed the expression of ECA1, MIZ1, and the miz1 mutant in the relevant yeast transformants (*SI Appendix*, Fig. S8*B*). These results suggest that MIZ1 has an inhibitory effect on ECA1 function, consistent with the *in planta* interaction of the two proteins (Fig. 5 *B* and *C*). Finally, to determine whether the MIZ1/ECA1 mechanism functions in the root tip, we quantified the $[Ca^{2+}]_{cyt}$ in root tips (the specific examined root tip part is indicated in *SI Appendix*, Fig. S1*C*) of Col-0, *miz1*, and *eca1-3* under control conditions and following 1 h of hydrostimulation. The levels of $[Ca^{2+}]_{cyt}$ in the root tips of *miz1* did not change appreciably in response to hydrostimulation and did not exceed the levels in Col-0 under control conditions (*SI Appendix*, Fig. S9). On the other hand, the $[Ca^{2+}]_{cyt}$ levels in the root tips of *eca1-3* were found to be higher than those of Col-0 under control conditions and to be slightly elevated in response to hydrostimulation (*SI Appendix*, Fig. S9). Collectively, these data suggest that both MIZ1 and ECA1 are required for generating the Ca^{2+} signal in the root tip in response to hydrostimulation.

Discussion

In this work, we revisited Darwin's assumption that a signal is transmitted from the root cap to the EZ in response to moisture differences across the root tip (1). Previously, forward genetics approaches revealed only two genes (*MIZ1* and *MIZ2*) mediating hydrotropism (24, 39); however, how the encoded proteins are involved in hydrotropism is not yet understood. We demonstrate

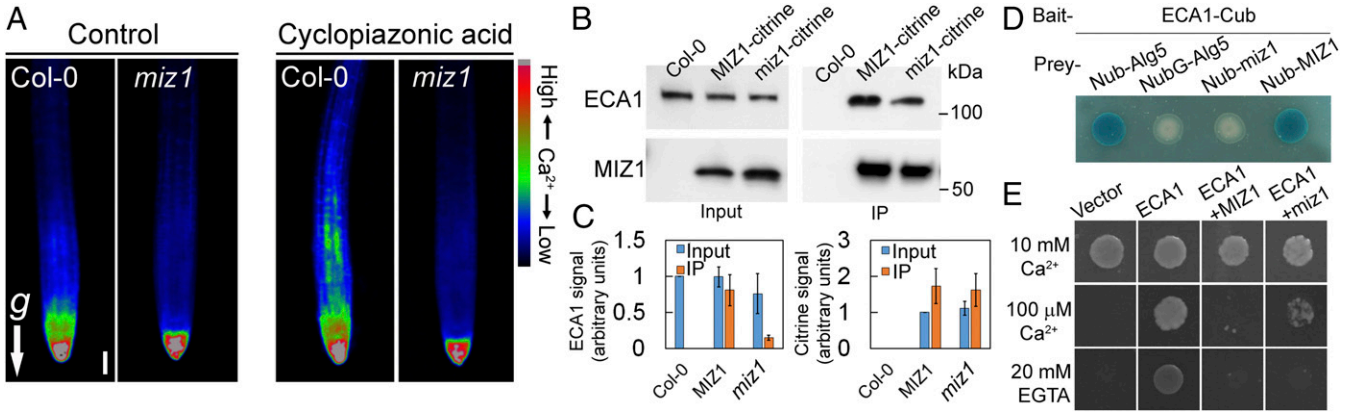

Fig. 5. Direct interaction between ECA1 and MIZ1 facilitates hydrotropic $[Ca^{2+}]_{cyt}$ signaling. (*A*) Confocal microscope visualization of NES-YC3.6 signals in roots of Col-0 and *miz1* roots treated with 0 (control) or 10 μM CPA for 1 h. *g* represents gravity vector. (Scale bar, 50 μm.) (*B* and *C*) Immunoprecipitation assay. (*B*) Microsomal membranes were isolated from 5-d-old whole seedlings expressing the MIZ1-citrine or miz1-citrine (Input), and protein was purified using GFP isolation kit (IP), followed by Western blot analysis with anti-ECA1 (38) or anti-GFP antisera. (*C*) Quantification of ECA1 and citrine signals. Error bars represent mean ± SD (three biological experiments). (*D*) Split-ubiquitin yeast two-hybrid assay. Vectors harboring ECA1 fused to the ubiquitin C terminus coding sequence (ECA1-Cub) and MIZ1 or miz1 fused to ubiquitin N terminus coding sequence were cotransformed to NMY51 *Saccharomyces cerevisiae* strain on selective medium supplemented with X-gal for detection of β-galactosidase activity. For positive and negative controls, cotransformation was performed with pAI-Alg5 (Nub-Alg5) or pDL2-Alg5 (NubG-Alg5, mutated Nub), respectively (*SI Appendix, Materials and Methods*). (*E*) Yeast growth complementation assay (*SI Appendix, Materials and Methods*). *S. cerevisiae* strain K616 was transformed with empty pESC-URA vector or with the vector harboring ECA1, ECA1 plus MIZ1, or ECA1 plus miz1, and spotted onto SG-URA plates supplemented with 10 mM $CaCl_2$ (Ca^{2+}, not selective), 100 μM $CaCl_2$ (selective), or 20 mM EGTA (highly selective). Representative results are from six independent drop tests with at least four independent biological samples. Expression of the proteins described in *D* and *E* are shown in *SI Appendix*, Fig. S8.

that root curvature in response to hydrostimulation requires long-distance $[Ca^{2+}]_{cyt}$ mobilization from the root cap to the EZ (Figs. 1 and 3 and *SI Appendix*, Figs. S1 and S9) that is mediated by the interaction of MIZ1 with the type 2A Ca^{2+}-ATPase isoform ECA1, an ER-localized Ca^{2+} efflux carrier. Furthermore, we provide evidence for the importance of the root tip in generating the hydrostimulated long-distance Ca^{2+} signal through the interaction of these proteins (*SI Appendix*, Fig. S1). The expression pattern of ECA1 and MIZ1 in the root tip, stele, and peripheral tissues of the EZ (*SI Appendix*, Fig. S7) (25, 40, 41) raises the possibility of an active MIZ1/ECA1 mechanism in different root tissues. However, the mechanism that underlies the propagation of the long-distance hydrotropic-driven $[Ca^{2+}]_{cyt}$ signal remains unknown. $[Ca^{2+}]_{cyt}$ propagation may involve other intermediate signals such as ROS or electric signals, as described for long-distance $[Ca^{2+}]_{cyt}$ signals associated with different physiological responses (27, 42, 43). We show that such Ca^{2+} signals do not occur in the *miz1* mutant (Fig. 1 *A* and *B* and *SI Appendix*, Fig. S3). Importantly, we found that in response to cross-root water potential differences, the long-distance Ca^{2+} signal is transmitted asymmetrically through the phloem to the EZ where it is laterally distributed asymmetrically to peripheral cells (Figs. 1 and 3 *A*, *C*, and *D*), and where it most likely promotes differential cell elongation underlying curvature. Furthermore, manipulations of $[Ca^{2+}]_{cyt}$ confirmed that transient elevation of $[Ca^{2+}]_{cyt}$ is required for root curvature toward water. Specifically, in the absence of the functional ER-localized Ca^{2+}-ATPase pump ECA1, $[Ca^{2+}]_{cyt}$ levels are elevated (Fig. 4*G* and *SI Appendix*, Fig. S6) and root curvature toward water is enhanced (Fig. 4 *E* and *F*). The role of the ER in regulating the homeostasis of $[Ca^{2+}]_{cyt}$ is reminiscent of the previously reported elevation of $[Ca^{2+}]_{cyt}$ levels in tobacco plants in which the type 2B ER-localized Ca^{2+}-ATPase NbCA1 was silenced, resulting in an enhanced hypersensitive immune response (44). Recently, the lack or overexpression of the ER-localized CCX2 (a Ca^{2+}/cation exchanger) was found to affect both cytosolic and ER Ca^{2+} dynamics and tolerance to salt and osmotic stress, demonstrating a role for the ER Ca^{2+} reservoir in the regulation of $[Ca^{2+}]_{cyt}$ homeostasis (45). Furthermore, our study provides several lines of evidence for the regulation of ECA1 by MIZ1. First, CPA, a known inhibitor of ECA1, was unable to inhibit ECA1 in a *miz1* mutant (Fig. 5*A*), suggesting that MIZ1 is associated with ECA1. Indeed, coimmunoprecipitation experiments confirmed this association (Fig. 5 *B* and *C*). Furthermore, protein–protein interaction assays in yeast revealed the direct interaction of ECA1 with MIZ1 but not with the miz1 mutant protein (Fig. 5*D*), which *in planta* abrogates hydrotropism (24). However, although ECA1 appears to function as a major player in the mechanism of root hydrotropism, the involvement of other Ca^{2+} transporters and/or channels, which function in maintaining $[Ca^{2+}]_{cyt}$ homeostasis or in generating a change from homeostasis in response to a signal, could not be ruled out. Collectively, these results raised the possibility that MIZ1 is a negative regulator of ECA1 and that the interaction of MIZ1 with ECA1 is essential for elevating $[Ca^{2+}]_{cyt}$ levels, which underlies root hydrotropic curvature. To test this, we employed a previously described functional complementation assay of yeast strain K616 by expression of ECA1 (35, 38). The results confirmed the ability of MIZ1, and to a much lesser extent miz1, to attenuate the complementation of yeast strain K616 by ECA1 (Fig. 5*E*), consistent with the proposed inhibitory effect of MIZ1 on ECA1 function. The experimental evidence demonstrating a mechanism underlying the elevation of $[Ca^{2+}]_{cyt}$ levels by inhibition of an ER type 2A Ca^{2+}-ATPase is unique, yet is consistent with the previously reported elevation of $[Ca^{2+}]_{cyt}$ levels resulting from artificially silencing a tobacco ER-localized type 2B Ca^{2+} ATPase (44). The simultaneous decline of $[Ca^{2+}]_{ER}$ and the elevation of $[Ca^{2+}]_{cyt}$ levels in the root tip upon hydrostimulation (*SI Appendix*, Fig. S1) further support this scenario. Hence, our study offers an example of a long-distance Ca^{2+} signal that is generated by inhibiting a Ca^{2+} efflux carrier, in agreement with previous theoretical considerations of the essential role of Ca^{2+} efflux carriers in stress signaling (46).

Another important question that we addressed is the spatial distribution of $[Ca^{2+}]_{cyt}$ reaching the EZ. We used light-sheet fluorescence microscopy to obtain an image of $[Ca^{2+}]_{cyt}$ distribution across the root in response to hydrostimulation. Remarkably, in response to hydrostimulation, $[Ca^{2+}]_{cyt}$ was

distributed asymmetrically across the root at the EZ, suggesting that this asymmetric distribution may facilitate asymmetric root cell elongation that results in root curvature. However, the mechanism downstream of this Ca^{2+} signal remains to be identified. The possible involvement of ABA in this Ca^{2+} effect cannot be ruled out (6).

However, several open questions regarding hydrotropism still remain unanswered. How is a water potential gradient across the root detected? How does the detector transduce the sensed water potential gradient to MIZ1 to generate an asymmetric Ca^{2+} signal? How does $[Ca^{2+}]_{cyt}$ propagate from the root tip to the EZ? How is the Ca^{2+} signal mobilized across the root at the EZ? Finally, how does asymmetric $[Ca^{2+}]_{cyt}$, which is distributed across the root, mediate asymmetric cell elongation and root curvature? Further interdisciplinary investigations are required to answer these open questions.

Materials and Methods

Plant materials, methodologies of microscopy work, yeast two-hybrid system, yeast functional complementation assays, and biochemical procedures are described in *SI Appendix*.

ACKNOWLEDGMENTS. We thank Prof. Heven Sze (University of Maryland) for kindly providing anti-ECA1 antibodies, Dr. Yoseph Addadi (Life Sciences Core Facilities, Weizmann Institute of Science) for help with light-sheet fluorescence microscopy, and Dr. Laura Luoni (Department of Biosciences, University of Milan) for generating the *eca1-3*/NES-YC3.6 lines. This research was supported by the Israeli Centers for Research Excellence Program of the Planning and Budgeting Committee, Israel Science Foundation Grant 757/12 (to H.F.), and Piano di Sviluppo di Ateneo, UMIL 2015 and 2016 (to A.C.).

1. Darwin C, Darwin F (1880) *The Power of Movement in Plants* (John Murray, London), pp 572–574.
2. Von Sachs J (1887) Lecture XXVII. Relations between growth and cell-division in the embryonic tissues. *Lectures on the Physiology of Plants* (Clarendon, Oxford), pp 431–459.
3. Jaffe MJ, Takahashi H, Biro RL (1985) A pea mutant for the study of hydrotropism in roots. *Science* 230:445–447.
4. Miyazawa Y, et al. (2008) Effects of locally targeted heavy-ion and laser microbeam on root hydrotropism in *Arabidopsis thaliana*. *J Radiat Res (Tokyo)* 49:373–379.
5. Antoni R, et al. (2013) PYRABACTIN RESISTANCE1-LIKE8 plays an important role for the regulation of abscisic acid signaling in root. *Plant Physiol* 161:931–941.
6. Dietrich D, et al. (2017) Root hydrotropism is controlled via a cortex-specific growth mechanism. *Nat Plants* 3:17057.
7. Iino M, Haga K (2005) Roles played by auxin in phototropism and photomorphogenesis. *Light Sensing in Plants* (Springer, Tokyo), pp 269–276.
8. Sato EM, Hijazi H, Bennett MJ, Vissenberg K, Swarup R (2015) New insights into root gravitropic signalling. *J Exp Bot* 66:2155–2165.
9. Band LR, et al. (2012) Root gravitropism is regulated by a transient lateral auxin gradient controlled by a tipping-point mechanism. *Proc Natl Acad Sci USA* 109: 4668–4673.
10. Kaneyasu T, et al. (2007) Auxin response, but not its polar transport, plays a role in hydrotropism of *Arabidopsis* roots. *J Exp Bot* 58:1143–1150.
11. Shkolnik D, Krieger G, Nuriel R, Fromm H (2016) Hydrotropism: Root bending does not require auxin redistribution. *Mol Plant* 9:757–759.
12. Joo JH, Bae YS, Lee JS (2001) Role of auxin-induced reactive oxygen species in root gravitropism. *Plant Physiol* 126:1055–1060.
13. Krieger G, Shkolnik D, Miller G, Fromm H (2016) Reactive oxygen species tune root tropic responses. *Plant Physiol* 172:1209–1220.
14. Choi WG, Toyota M, Kim S-H, Hilleary R, Gilroy S (2014) Salt stress-induced Ca^{2+} waves are associated with rapid, long-distance root-to-shoot signaling in plants. *Proc Natl Acad Sci USA* 111:6497–6502.
15. Gilroy S, et al. (2014) A tidal wave of signals: Calcium and ROS at the forefront of rapid systemic signaling. *Trends Plant Sci* 19:623–630.
16. van Bel AJE, et al. (2014) Spread the news: Systemic dissemination and local impact of Ca^{2+} signals along the phloem pathway. *J Exp Bot* 65:1761–1787.
17. Takano M, Takahashi H, Suge H (1997) Calcium requirement for the induction of hydrotropism and enhancement of calcium-induced curvature by water stress in primary roots of pea, *Pisum sativum* L. *Plant Cell Physiol* 38:385–391.
18. Miao R, et al. (2018) Comparative analysis of *Arabidopsis* ecotypes reveals a role for brassinosteroids in root hydrotropism. *Plant Physiol* 176:2720–2736.
19. Lee JS, Mulkey TJ, Evans ML (1983) Reversible loss of gravitropic sensitivity in maize roots after tip application of calcium chelators. *Science* 220:1375–1376.
20. Monshausen GB, Messerli MA, Gilroy S (2008) Imaging of the Yellow Cameleon 3.6 indicator reveals that elevations in cytosolic Ca^{2+} follow oscillating increases in growth in root hairs of *Arabidopsis*. *Plant Physiol* 147:1690–1698.
21. Li J, et al. (2011) MDP25, a novel calcium regulatory protein, mediates hypocotyl cell elongation by destabilizing cortical microtubules in *Arabidopsis*. *Plant Cell* 23: 4411–4427.
22. Iwano M, et al. (2009) Fine-tuning of the cytoplasmic Ca^{2+} concentration is essential for pollen tube growth. *Plant Physiol* 150:1322–1334.
23. Krebs M, et al. (2012) FRET-based genetically encoded sensors allow high-resolution live cell imaging of Ca^{2+} dynamics. *Plant J* 69:181–192.
24. Kobayashi A, et al. (2007) A gene essential for hydrotropism in roots. *Proc Natl Acad Sci USA* 104:4724–4729.
25. Yamazaki T, et al. (2012) MIZ1, an essential protein for root hydrotropism, is associated with the cytoplasmic face of the endoplasmic reticulum membrane in *Arabidopsis* root cells. *FEBS Lett* 586:398–402.
26. Bonza MC, et al. (2013) Analyses of Ca^{2+} accumulation and dynamics in the endoplasmic reticulum of *Arabidopsis* root cells using a genetically encoded Cameleon sensor. *Plant Physiol* 163:1230–1241.
27. Evans MJ, Choi WG, Gilroy S, Morris RJ (2016) A ROS-assisted calcium wave dependent on AtRBOHD and TPC1 propagates the systemic response to salt stress in *Arabidopsis* roots. *Plant Physiol* 171:1771–1784.
28. Cramer GR, Jones RL (1996) Osmotic stress and abscisic acid reduce cytosolic calcium activities in roots of *Arabidopsis thaliana*. *Plant Cell Environ* 19:1291–1298.
29. Eckardt NA (2001) A calcium-regulated gatekeeper in phloem sieve tubes. *Plant Cell* 13:989–992.
30. Candeo A, Doccula FG, Valentini G, Bassi A, Costa A (2017) Light sheet fluorescence microscopy quantifies calcium oscillations in root hairs of *Arabidopsis thaliana*. *Plant Cell Physiol* 58:1161–1172.
31. McLean BG, Hempel FD, Zambryski PC (1997) Plant intercellular communication via plasmodesmata. *Plant Cell* 9:1043–1054.
32. Wright KM, Oparka KJ (1997) Metabolic inhibitors induce symplastic movement of solutes from the transport phloem of *Arabidopsis* roots. *J Exp Bot* 48:1807–1814.
33. Takahashi N, Goto N, Okada K, Takahashi H (2002) Hydrotropism in abscisic acid, wavy, and gravitropic mutants of *Arabidopsis thaliana*. *Planta* 216:203–211.
34. Antoni R, Dietrich D, Bennett MJ, Rodriguez PL (2016) Hydrotropism: Analysis of the root response to a moisture gradient. *Methods Mol Biol* 1398:3–9.
35. Liang F, Sze H (1998) A high-affinity Ca^{2+} pump, ECA1, from the endoplasmic reticulum is inhibited by cyclopiazonic acid but not by thapsigargin. *Plant Physiol* 118: 817–825.
36. Bonza MC, De Michelis MI (2011) The plant Ca^{2+}-ATPase repertoire: Biochemical features and physiological functions. *Plant Biol (Stuttg)* 13:421–430.
37. Cunningham KW, Fink GR (1994) Calcineurin-dependent growth control in *S. cerevisiae* mutants lacking PMC1, a homolog of plasma membrane calcium ATPase. *J Cell Biol* 124: 351–363.
38. Liang F, Cunningham KW, Harper JF, Sze H (1997) ECA1 complements yeast mutants defective in Ca^{2+} pumps and encodes an endoplasmic reticulum-type Ca^{2+}-ATPase in *Arabidopsis thaliana*. *Proc Natl Acad Sci USA* 94:8579–8584.
39. Miyazawa Y, et al. (2009) GNOM-mediated vesicular trafficking plays an essential role in hydrotropism of *Arabidopsis* roots. *Plant Physiol* 149:835–840.
40. Moriwaki T, Miyazawa Y, Fujii N, Takahashi H (2012) Light and abscisic acid signalling are integrated by MIZ1 gene expression and regulate hydrotropic response in roots of *Arabidopsis thaliana*. *Plant Cell Environ* 35:1359–1368.
41. Moriwaki T, et al. (2011) Hormonal regulation of lateral root development in *Arabidopsis* modulated by MIZ1 and requirement of GNOM activity for MIZ1 function. *Plant Physiol* 157:1209–1220.
42. Choi WG, Hilleary R, Swanson SJ, Kim S-H, Gilroy S (2016) Rapid, long-distance electrical and calcium signaling in plants. *Annu Rev Plant Biol* 67:287–307.
43. Mittler R, et al. (2011) ROS signaling: The new wave? *Trends Plant Sci* 16:300–309.
44. Zhu X, Caplan J, Mamillapalli P, Czymmek K, Dinesh-Kumar SP (2010) Function of endoplasmic reticulum calcium ATPase in innate immunity-mediated programmed cell death. *EMBO J* 29:1007–1018.
45. Corso M, Doccula FG, de Melo JRF, Costa A, Verbruggen N (2018) Endoplasmic reticulum-localized CCX2 is required for osmotolerance by regulating ER and cytosolic Ca^{2+} dynamics in *Arabidopsis*. *Proc Natl Acad Sci USA* 115:3966–3971.
46. Bose J, Pottosin II, Shabala SS, Palmgren MG, Shabala S (2011) Calcium efflux systems in stress signaling and adaptation in plants. *Front Plant Sci* 2:85.